ELSEVIER

Ceramics International 31 (2005) 989–997

CERAMICS INTERNATIONAL

www.elsevier.com/locate/ceramint

Charge compensation mechanism in yttria-doped barium titanate

Hong-Yang Lu*, Ming-Hong Lin[1]

Centre for Nanoscience, Institute of Materials Science and Engineering, National Sun Yat-Sen University, Kaohsiung 80424, Taiwan

Received 26 January 2004; received in revised form 30 September 2004; accepted 15 October 2004
Available online 12 January 2005

Abstract

A commercial TiO_2-excess $BaTiO_3$ powder doped with Y_2O_3 has been pressureless-sintered using conventional tube furnace and CO_2-laser, and the room-temperature electrical conductivity determined. Grain-growth inhibition is found to occur at ~0.40 mol% Y_2O_3 where the refined microstructure of an average grain size of ~1 μm is obtained from sintering at 1215 °C. The principal charge compensation mechanism in Y_2O_3-doped $BaTiO_3$ depending upon temperature can be divided into three characteristic regimes. The mechanism is predominantly of the cation vacancy compensation at temperatures <1210 °C, a mixed mode at 1210–1500 °C, and the electron compensation when sintering temperature exceeds 1500 °C. Sintering using the CO_2-laser has enabled the retention of the high temperature defect equilibrium which renders the room-temperature conductivity of $\sim 10^{-2}\ (\Omega\ \mathrm{mm})^{-1}$ to the ceramics. The sintering of Y_2O_3-doped $BaTiO_3$ ceramics is improved since densification is enhanced by faster barium diffusion via the extrinsic cation vacancy and coarsening suppressed by high Y_2O_3-content due to reduced grain-boundary mobility by second-phase ($Y_2Ti_2O_7$) pinning.

Keywords: A. Sintering; B. Defects; B. Microstructure-final; C. Electrical conductivity; D. $BaTiO_3$ and titanates

1. Introduction

A cation vacancy mechanism for principal charge compensation is usually taken to argue for enhanced densification in donor-doped $BaTiO_3$ ceramics observed experimentally in the solid-state sintering [1,2]. Effective grain-growth inhibition for donor-doping occurs between ~0.20 and 0.40 mol% such as La_2O_3 [1,2], and Sb_2O_3 [3]. The lower donor concentration has been conveniently termed the grain-growth inhibition threshold (GGIT) [4]. The sintering of $BaTiO_3$ ceramics is enhanced and the microstructure refined simultaneously to an average grain size (G_{av}) of ~1–3 μm with dopant content exceeds GGIT. However, eutectic liquids [5,6] forming at temperatures below 1350 °C [1,2] have interfered with the interpretation of the sintering kinetic data [6], arguing for densification enhancement in the solid state. Furthermore, the ceramics with donor–dopants in this range had low electrical conductivities, often became insulators [1].

The coincidence of the room-temperature conductivity maximum and the onset of grain-growth inhibition suggested [1] a correlation between the vacancy compensation and grain-growth control. It was postulated [7] that the barium vacancy (V''_{Ba}) [6] formed upon cooling in an oxidising atmosphere is the most important intrinsic defect. The principal charge compensation defect being V''_{Ba} was implied and later considered [8] to be kinetically more mobile, although others [9] have indicated that the formation of the titanium vacancy was favourable thermodynamically. In fact, an enrichment of Ti relative to Ba was found [10] on the surface of slowly cooled Nb-doped $BaTiO_3$ ceramics, indicating excessive barium vacancies on the surface. It was suggested [7] that the principal charge compensation mechanism depends upon the temperature and the oxygen partial pressure, p_{O_2}, in the sintering atmosphere. The overall charge neutrality in the ceramics is maintained by a mixture of cation vacancy and electron, i.e. mixed mode, regardless of the donor oxide and its concentration [1,2,7].

More specifically, the principal charge compensation mechanism of three distinctive schemes, depending on the sintering temperature (T) for donor-doped $BaTiO_3$ sintered

* Corresponding author. Fax: +886 7 5256030.
E-mail address: hyl@mail.nsysu.edu.tw (H.-Y. Lu).
[1] Present address: Department of Mechanical Engineering, National Kaohsiung University of Applied Sciences, Kaohsiung 80728, Taiwan.

0272-8842/$30.00
doi:10.1016/j.ceramint.2004.10.014

and cooled to room temperature in air was proposed before [3,7]. It is summarised below,

(I)	$T < 1220$ °C	$N_D \approx 2[V''_{Ba}]$	Vacancy compensation
(II)	1220 °C $< T <$ 1500 °C	$N_D = 2[V''_{Ba}] + n$	Mixed mode
(III)	$T > 1500$ °C	$N_D \approx n$	Electron compensation

where N_D is the concentration of donor cation and n is the concentration of electron.

Yet, donor-doped $BaTiO_3$ sintered at 1220–1500 °C in air has produced semiconductors as well as insulators [1,2,7]. Thus, a kinetically controlled mechanism of equilibrium restoration has been proposed to account for the limited electrical conductivity of donor-doped $BaTiO_3$ at room temperature [3,7]. The ability to restore equilibrium upon cooling is determined kinetically by the diffusion of barium vacancy inwards to the grain interior from surface. Defect distribution depending on the cooling rate is inhomogeneous across the grains and each grain would have contained a rim of barium vacancy with frozen-in defects in the grain interior. However, the proposed temperature-dependent charge compensation regimes have not been verified experimentally.

In a preliminary study of the Y_2O_3-doped $BaTiO_3$ compositions sintered at 1350 °C, a large discrepancy of the electrical conductivity by $\sim 10^5$ was found in the ceramics of similarly refined microstructure with an average grain size $G_{av} \approx 15$–18 μm. It demonstrates that laser sintering has produced $BaTiO_3$ ceramics with significantly higher electrical conductivity at room temperature. The fast cooling rate from sintering temperatures afforded by CO_2-laser appears to be a determining factor. The implication is that the room-temperature conductivity is determined by a kinetic process [3,7] occurred upon cooling from sintering temperatures. We have, therefore, studied the room-temperature electrical conductivity of $BaTiO_3$ ceramics doped with Y_2O_3 adopting pressureless-sintering technique of two vastly different cooling rates. The conductivity data reported here confirm the existence of the three-charge compensation regimes proposed by Wernicke [3] and Daniels [7].

2. Experimental procedure

A commercial TiO_2-excess 0.997 nonstoichiometric $BaTiO_3$ powder (Ticon® HPB) supplied by Ferro (Penn Yan, NY, USA) was used in this study. Reagent grade $Y(NO_3)_3 \cdot 6H_2O$ (Merck, Darmstadt, Germany) was mixed with 1 wt% polyvinyl butyral (PVB) binder in absolute alcohol before milling in a polypropylene (PP) jar with nylon-coated steel balls for 2 h. The mixed slurry was oven-dried, de-agglomerated using an agate mortar and pestle, then passed through a ~74 μm mesh. An appropriate amount of powder was die-pressed to discs of 5 mm in diameter in a WC-inserted steel die by applying uniaxial pressure of 100 MPa. Samples were then sintered in a conventional tube furnace by the heating rate of 5 °C min^{-1} or using a CO_2-laser (PRC, FH-3000, Landing, NJ, USA). The experimental detail of adopting CO_2-laser for sintering was reported before [11].

Sintered density was determined by applying the Archimedes technique when distilled water was used as the immersion medium. Sintering kinetic curves are established by plotting the final sintered density against sintering time. The room-temperature electrical conductivity was determined using a two-point probe on polished sample surface coated with In–Ga electrodes using an electrometer (model 617, Keithley, Cleveland, OH, USA).

Sintered samples were mechanically ground and polished with SiC grits successively before diamond lapping to 1 μm surface roughness for microstructure observation. Grain-boundaries were delineated with thermal etching at 1200 °C, or chemical etching using 1% HF solution where appropriately. Average grain size was determined on SEM micrographs, taken from JEM6400 (JEOL, Tokyo, Japan), adopting the linear intercept technique [12]. Thin foils for TEM were prepared by the standard procedures of slicing, ultrasonic drilling, polishing followed by dimple grinding and Ar^+-beam thinning to electron transparency. Observations were performed in a JEOL AEM3010 operating at 300 kV.

3. Results

3.1. Sintering behaviour and microstructures

Fig. 1 shows the sintering curves of Y_2O_3-doped $BaTiO_3$ by furnace-sintering at 1215 °C for up to 150 h. Sintering of the ceramics has been improved and higher final density (described in relative density, ρ_{rel}) obtained by donor-doping. An increase of $\Delta\rho_{rel} \approx 16\%$ was obtained by adding 0.80 mol% Y_2O_3. However, it also appears that the sintered density was improved only insignificantly with Y_2O_3-doping

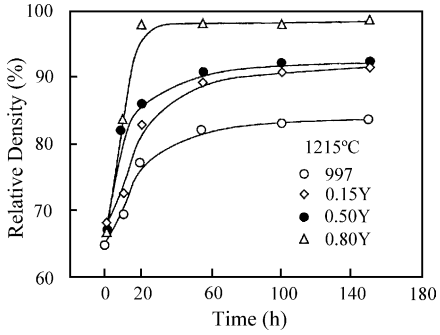

Fig. 1. Sintering curves for Y_2O_3-doped $BaTiO_3$ by furnace sintering at 1215 °C up to 150 h.

between 0.15 and 0.50 mol%. The sudden increase of final sintered density from the undoped to 0.15 mol% doped samples, and again from the 0.50 to 0.80 mol% doped samples can easily be discerned (Fig. 1). The increasing trend differs characteristically from that reported [11] for the La_2O_3-doped samples where the sintered density increased progressively with the dopant concentration.

Pressureless-sintering of doped samples containing $Y_2O_3 < 0.30$ mol% at low temperatures (1215 °C for 100 h) in a conventional furnace produced a bimodal

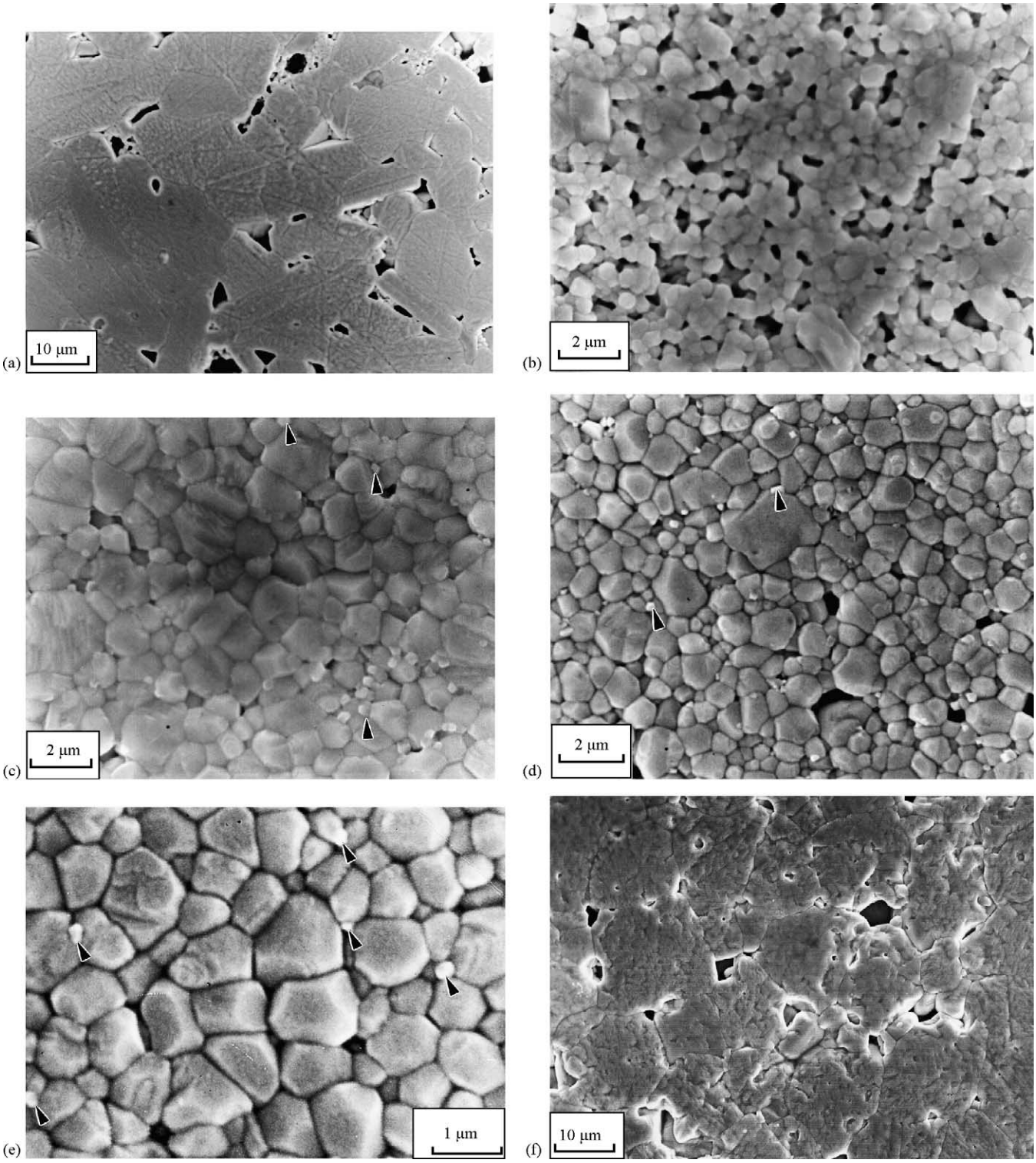

Fig. 2. Microstructures of Y_2O_3-doped $BaTiO_3$: (a) 0.30 mol%, (b) 0.40 mol%, (c) 0.80 mol% pressureless-sintered at 1215 °C for 100 h, (d) 0.80 mol% laser-sintered at 1450 °C for 60 s, (e) 1.0 mol% Y_2O_3 pressureless-sintered at 1300 °C for 15 h, and (f) 0.15 mol% Y_2O_3 laser-sintered at 1450 °C for 60 s (SEM-SEI).

grain-size microstructure. It consists of large plate-like grains, forming a skeletal network (Fig. 2a), with intergranularly located small grains [13–15]. This is the representative microstructure of the undoped TiO_2-excess $BaTiO_3$ [6]. The skeletal microstructure hinders further densification [6] and facetted residual pores are readily discerned (e.g. Fig. 2a). Similar microstructure persists until the dopant level has exceeded 0.30 mol% (referred to Fig. 2b for 0.40 mol%). The indication is that grain-growth inhibition requires a critical dopant concentration to become effective [1,4]. The most striking evidence is the drastic modification of the sintered microstructure when Y_2O_3-dopant level increased from 0.30 mol% (Fig. 2a) to 0.40 mol% (Fig. 2b). Growth of plate-like grains (Fig. 2b) was completely arrested. The microstructure is altered abruptly from the skeletal network to one consisted of refined grains with homogeneous grain-size distribution. Intergranularly located ''second-phase'' particles, similar to $La_2Ti_2O_7$ in La_2O_3-doped [11] and $Er_2Ti_2O_7$ in Er_2O_3-doped samples [16], are observed, as indicated in Fig. 2c–e. This ''second-phase'' later identified to be $Y_2Ti_2O_7$ by TEM (Fig. 3) in fact starts to appear in samples with dopant

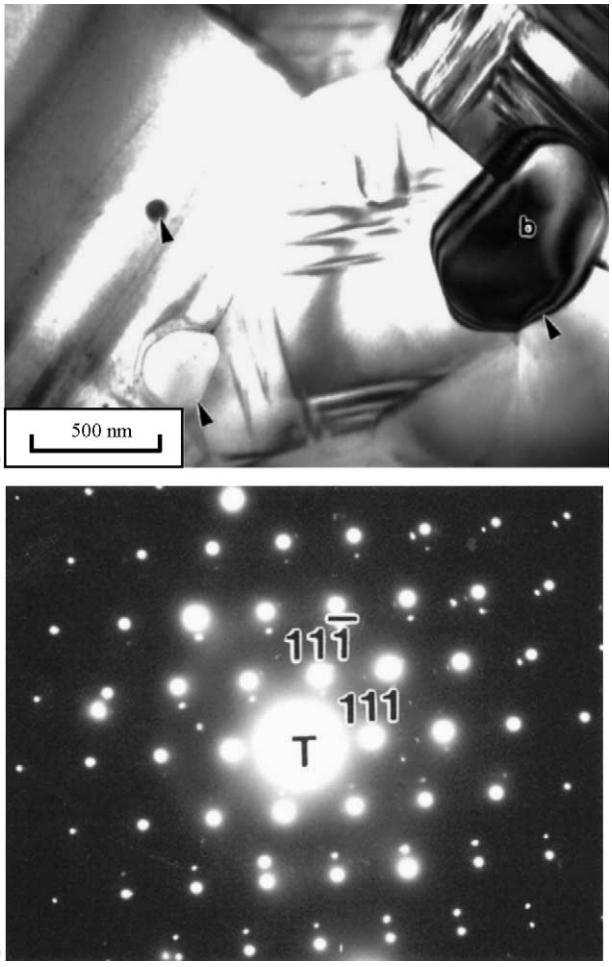

Fig. 3. Second-phase (as indicated) in 1.0 mol% Y_2O_3-doped samples from sintering at 1300 °C for 15 h: (a) BF image and (b) the corresponding SADP ($Z = [\bar{1}\ 1\ 0]$) (TEM).

level higher than 0.80 mol% Y_2O_3. It is discernible from the 1.0 mol% Y_2O_3-doped sample sintered at 1300 °C for 15 h and shown in Fig. 3a where those intergranularly located particles do not exhibit ferroelectric domain contrast upon rigorous tilting in the microscope.

A representative microstructure for samples doped with 0.15 mol% Y_2O_3, and laser-sintered at 1450 °C for 60 s is shown in Fig. 2f for comparison. Although plate-like grains have disappeared [11] due to sintering at a higher temperature, it is distinctive that grains have become polygonal in shape [4] and grown appreciably comparing to those shown in Fig. 2a.

Grain (**b**) with the corresponding SADP given in Fig. 3b can be indexed to $Y_2Ti_2O_7$ ($Y_2O_3{\cdot}2TiO_2$) of the cubic symmetry (JCPDS 27-982). Unlike the elongated $La_2Ti_2O_7$ [11] and $Er_2Ti_2O_7$ [16] grains located along $BaTiO_3$ grain-boundaries, three different sizes of second-phase particles are observed in Fig. 3a, as indicated by arrows. The smallest one of ~50 nm has apparently been swept across by moving boundary and become entrapped in the grain interior [17]. This particular second-phase was also identified by XRD in Y_2O_3-doped TiO_2-excess $BaTiO_3$ by Blanchart et al. [18]. The indication is that the 1.0 mol% Y_2O_3 dopant, similar to 2.0 mol% Er_2O_3 [16], was not completely dissolved at 1300 °C in the solid state. Similar to the La_2O_3-doped samples [11], some of the Y_2O_3 has reacted with the excess TiO_2 during sintering [11,19,20].

It is the first time that the grain-growth inhibition in $BaTiO_3$ by donor-doping is unambiguously demonstrated at 1215 °C, below the known eutectic liquids, 1250 and 1332 °C [5]. This represents unequivocally that the inhibition has occurred in solid-state sintering.

For doping with Y_2O_3 less than 0.40 mol%, the sintered microstructure depends strongly on the sintering temperature. Abnormally grown grains of the polygonal shape have dominated the microstructure development for samples sintered at above 1332 °C. When dopant level exceeds GGIT (>0.40 mol% Y_2O_3, shown in Fig. 2b–e), sintered samples are characterised by the refined and homogeneous microstructure of $G_{av} \approx 1.0$ μm irrespective of the sintering temperatures being below or above the lowest eutectic point 1332 °C in the BaO–TiO_2 binary (e.g. Fig. 2b showing samples with 0.40 mol% Y_2O_3 and Fig. 2c with 0.80 mol% sintered at 1215 °C, Fig. 2d with 0.80 mol% Y_2O_3, Fig. 2e with 1.0 mol% Y_2O_3, and Fig. 2f with 0.15 mol% Y_2O_3 at 1450 °C). An average grain size ~15 μm shown in Fig. 2f (comparing with ~1.0 μm in Fig. 2b) demonstrates that lightly doped samples are not effectively inhibited of grain growth.

Fig. 4 illustrates the critical temperature at which the average grain size of laser-sintered samples increases discontinuously. The temperature at which G_{av} increases abruptly also varies with the dopant content. That is deferred to higher temperatures with increasing Y_2O_3-doping, e.g. ~1310 °C for 0.15 mol% Y_2O_3 and ~1480 °C for 0.80 mol% Y_2O_3.

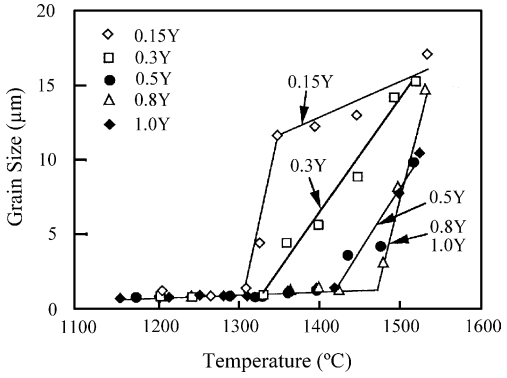

Fig. 4. Abrupt increase of average grain size in Y_2O_3-doped samples sintered using CO_2-laser.

3.2. Electrical conductivity of as-sintered samples

Samples were laser-sintered at 1200–1525 °C for 60 s followed by rapid cooling to room temperature, referred as the ''quenched'' samples by Daniels [7]. Laser sintering [11] normally takes less than 30 s for samples to cool down to room temperature, therefore, enables investigation into the high-temperature defect equilibrium retained to room temperature in ''air-quenched'' samples.

The electrical conductivity (σ) at room temperature is shown in Fig. 5a for samples doped with four Y_2O_3 contents. Three distinctive regions [7] labelled (I), (II) and (III) may be identified. For samples doped with 0.15 mol% Y_2O_3, the conductivity was approximately one order of magnitude higher than those of the others (doped with 0.30, 0.80, and 1.0 mol%) for sintering at >1265 °C (T_1). They are described below.

Region (I): Conductivity remains almost constant for all samples sintered at $T < 1265$ °C. Charge compensation by cation vacancies is likely to be the predominant mechanism [7]. Nevertheless, electron compensation was not completely absent for the conductivity $\sigma \approx 8.0 \times 10^{-9}$ $(\Omega\ \text{mm})^{-1}$ (Fig. 5a) can still be measured by electrometer. A common transition temperature from predominantly cation vacancy compensation to a mixed scheme occurs at $T_1 \approx 1265$ °C for all samples with low and high doping levels.

Region (II): Two straight lines are almost in parallel. The indication is that electron compensation is gradually favoured and increases with higher sintering temperatures >1265 °C. A transition occurs at 1265 °C (designated T_1) where the conductivity increases discontinuously by $\sim 10^3$. The conductivity increases steadily with sintering temperature between 1265 °C $< T <$ 1365 °C where the 0.15 mol% samples are more conductive by ~10 times. The indication is that the electron concentration of the 0.15 mol% Y_2O_3-doped samples (the upper line) is 10 times higher than that of the others, other properties, e.g. electron mobility being the same. For higher Y_2O_3-doping levels (of 0.80 and 1.0 mol%), the dependence of electrical conductivity on temperature is parallel to samples with 0.15 mol% Y_2O_3.

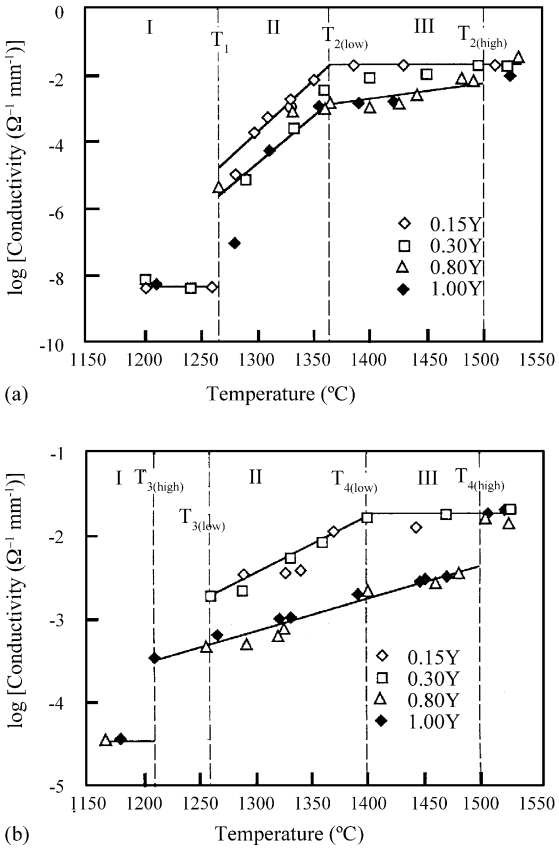

Fig. 5. Electrical conductivity vs. sintering temperature of (a) laser-sintered and (b) pressureless-sintered and post-annealed by CO_2-laser for Y_2O_3-doped $BaTiO_3$ showing three defect compensation regimes.

This suggests that the concentration of charge-compensating electron increases with temperature at a similar rate irrespective of higher Y_2O_3-doping levels. The electrical conductivities of the 0.30 mol% Y_2O_3-doped samples are persistently higher than those of the others again by ~10 times until beyond >1500 °C in region (III). Nevertheless, the trend of increasing conductivity is decreased by six times (by comparing the respective slopes of the straight lines between $T_{2(low)}$ and $T_{2(high)}$) from temperatures of ≥1365 °C (designated $T_{2(low)}$), as described below.

Region (III): The conductivity of the 0.15 mol% Y_2O_3-doped samples has reached a plateau of $\sigma \approx 8.0 \times 10^{-1}$ $(\Omega\ \text{mm})^{-1}$ from 1365 °C (designated as $T_{2(low)}$ where (low) represents low doping levels) to 1525 °C. Electron compensation becomes the dominating mechanism for samples doped with 0.15 mol% Y_2O_3 and sintered at 1365–1525 °C where the conductivity remains almost unchanged. In fact, the conductivity has come to a fixed value (of $\sigma \approx 8.0 \times 10^{-1}$ $(\Omega\ \text{mm})^{-1}$) for all samples investigated (Fig. 5a) when sintered at 1525 °C. For samples doped with higher Y_2O_3 (of 0.80 and 1.0 mol%), a constant conductivity did not occur until $T_{2(high)} \approx 1500$ °C, where (high) represents high doping levels. It is found for higher donor-doping levels that the conductivity changes discontinuously to a constant value of $\sim 10^{-2}$ $(\Omega\ \text{mm})^{-1}$ only occurs

at $T \geq T_{2(high)}$ (1500 °C). The implication is that the principal charge compensation mechanism has abruptly altered to favour electron compensation at 1500 °C. The transition to predominantly electron compensation (region (III)) has been deferred to a higher temperature of $T_{2(high)} \sim 1500$ °C for samples of higher Y_2O_3-contents (versus $T_{2(low)} \sim 1365$ °C of lower Y_2O_3-contents). Samples with higher Y_2O_3 (i.e. 0.80 and 1.0 mol%) also experience a gradual transition of the principal charge compensation mechanism over a wider temperature range. It changes to predominantly electron compensation over a temperature range $\Delta T = 235$ °C (between 1265 °C (T_1) and 1500 °C ($T_{2(high)}$)), unlike the narrower range of $\Delta T = 100$ °C (between 1265 °C (T_1) and 1365 °C ($T_{2(low)}$)) for samples with lower doping levels.

For low Y_2O_3-doping of 0.15 mol%, the electron concentration is saturated at the much lower temperature of $T_{2(low)} = 1365$ °C. The transition from a mixed compensation of cation vacancy and electron to predominantly electron compensation occurs at $T_{2(low)} = 1365$ °C for samples containing lower doping levels (e.g. 0.15 mol%). The temperature at the transition (T_2) termed as the inversion temperature by Daniels [7] was deferred until $T_{2(high)} \approx 1500$ °C for higher Y_2O_3-doping levels of 0.30, 0.80 and 1.0 mol% (Fig. 5a). Conductivities in region (II) are resulted from a mixed compensation mechanism of electron and cation vacancy with electron compensation being progressively favoured upon increasing sintering temperature. The slope of increasing conductivity may also reflect the dissolution kinetics of Y^{3+}, depending on the temperature.

3.3. Semiconductivity of annealed samples

In order to improve the dissolution of Y_2O_3 in $BaTiO_3$, samples were pressureless-sintered in a conventional tube furnace before post-sintering annealed using CO_2-laser. Better dissolution of Y^{3+} in the solid state enables investigation into the high-temperature defect equilibrium.

For samples pressureless-sintered at 1300 °C for 15 h followed by post-annealing for 60 s, the conductivities are plotted against the annealing temperature in Fig. 5b. Three regions similar to Fig. 5a can again be distinguished. Each region corresponds to a specific neutrality approximation of electron and cation vacancy compensation that is strongly dependent upon the dopant concentration and the post-annealing temperature.

Region (I): The conductivity of $\sigma \approx 5.0 \times 10^{-4}$ $(\Omega\ mm)^{-1}$ was obtained at room temperature for sintering temperatures <1210 °C in samples with lower Y_2O_3-doping levels (of 0.15 and 0.30 mol%). Cation-vacancy compensation predominates in this region, but the corresponding temperature range is less extensive comparing with that of the laser-sintered samples (Fig. 5a). The transition temperature being lower at 1210 °C, designated $T_{3(high)}$ (where (high) again represents the high doping levels of 0.80 and 1.0 mol% Y_2O_3), indicates the abrupt transition to a mixed compensation scheme. However, the transition temperature $T_{3(low)}$ for lower doping levels (of 0.15 and 0.30 mol%) only emerges at 1265 °C with an extended region (I).

The conductivity is higher than those of the laser-sintered samples (Fig. 5a) in the same region of predominantly vacancy compensation by $\sim 4 \times 10^3$ times (i.e. 2×10^{-8} $(\Omega\ mm)^{-1}$ versus 5×10^{-4} $(\Omega\ mm)^{-1}$). It indicates that better dissolution of Y^{3+} in the solid state has permitted a higher concentration of the charge compensation electron. The transition from a mixed mode to predominantly electron compensation occurred at $T_{3(high)} = 1210$ °C for higher Y_2O_3-doping levels (of 0.80 and 1.0 mol%). It almost coincides with the inversion temperature of 1220 °C reported for La_2O_3-doping by Daniels [7].

Region (II): The conductivity of samples doped with 0.15 and 0.30 mol% Y_2O_3 increases at a faster rate (than that of the higher Y_2O_3-doped samples) in this region, but they only show conductivity from annealing at temperatures above the inversion temperature $T_{3(low)} = 1265$ °C. The samples were insulators from annealing at temperatures below 1265 °C. For low Y_2O_3-doping levels of 0.15 and 0.30 mol%, region (I) of temperatures below $T_{3(low)}$ was not detected at all. The conductivity, below $T_{3(low)}$, was beyond the range of the electrometer used here. It implies that Y_2O_3 dissolving into $BaTiO_3$ has generated only negligible concentration of conducting electron and the charge neutrality was achieved by cation vacancy below $T_{3(low)} = 1265$ °C (which is higher than that predicted by Daniels et al. for samples doped with La_2O_3). It is also that lower Y_2O_3 content exhibits a more extensive temperature range of the cation vacancy compensation scheme, i.e. until $T_{3(low)} = 1265$ °C. However, it reaches a conductivity plateau at $T_{4(low)} = 1400$ °C (designated $T_{4(low)}$ in Fig. 5b) sooner than that of samples with higher dopant contents. For higher Y_2O_3-contents of 0.80 and 1.0 mol%, conductivity increases steadily but at a slower rate in 1210 °C < T < 1500 °C. In that temperature range, charge compensation mechanism has altered from a mixed scheme to predominantly electron. Not until $T_{4(high)} = 1500$ °C does the transition to predominantly electron compensation take place with a distinctive discontinuity. The temperature range is more extensive where the inversion temperature [7] occurs at 1210 °C (designated $T_{3(high)}$) representing the transition from predominantly vacancy to a mixed compensation scheme.

Region (III): The conductivity of samples doped with 0.15 and 0.30 mol% Y_2O_3 remains constant at $\sigma \approx 8 \times 10^{-1}$ $(\Omega\ mm)^{-1}$ over 400 °C < T < 1525 °C. The temperature $T_{4(low)} = 1400$ °C is the temperature at which charge compensation clearly switches to predominantly electron. For samples doped with 0.80 and 1.0 mol% Y_2O_3, conductivity increases continuously from region (II) of $T_{3(high)} = 1210$ °C until reaching region (III) at $T_{4(high)} = 1500$ °C. The conductivities (of $\sim 8 \times 10^{-1}$ $(\Omega\ mm)^{-1}$) are identical to that of the samples with lower donor-doping. An abrupt change of conductivity occurs at 1500 °C ($T_{4(high)}$)

coinciding with that observed in Fig. 5a for as-sintered samples.

4. Discussion

4.1. Mechanism of grain-growth inhibition

The refined microstructure (Fig. 2b) where the plate-like grains have disappeared demonstrates unambiguously that grain-growth inhibition is effective by Y_2O_3-doping. The critical donor concentration of 0.40 mol% Y_2O_3 falls outside the GGIT of 0.20–0.30 mol% reported for La_2O_3-doping [1,4] when they are both donor cations of valence 3+. While the donor–acceptor self-compensation [1] from the (B-site) acceptor impurities, e.g. Al_2O_3 and Fe_2O_3, associated with the starting powder may account for the discrepancy, it is also due to the site-occupancy of Y^{3+} that substitutes for both the A- and B-cation sites in $BaTiO_3$ [8,19,20]. The site occupancy of rare-earth cations, e.g. Y^{3+}, Er^{3+}, Nd^{3+}, Dy^{3+}, and others being amphoteric, are known to depend on sintering temperature, Ba/Ti-ratio and oxygen partial pressure in the sintering atmosphere [21].

Grain-growth inhibition in donor-doped $BaTiO_3$ [2,8,22] has adopted [2,22] the argument of enhanced ($d\rho/dG$) ratio [23] in favour of a defect structure containing predominantly cation vacancy when densification is improved preferentially. Enhanced densification evidenced by the kinetics of solid-state sintering at 1215 °C (shown in Fig. 1) also supports this view. It is because of the higher concentration of extrinsic cation vacancies generated by donor-doping. Low conductivities for all samples below $T_1 = 1260$ °C (Fig. 5a) further supports charge compensation predominantly by vacancy with Y_2O_3-doping, for all doping levels studied here.

The argument [6] that barium lattice diffusion was rate determining for sintering was based on principal charge compensation by barium vacancies, at least kinetically [8] with donor-doping. The existence of second-phase along grain-boundaries in both La_2O_3 [11], Er_2O_3 [16] and Y_2O_3-doped samples ($Y_2Ti_2O_7$ (Fig. 3)) with high doping levels, however, suggests that the solid-solution defect theory is not the sole mechanism responsible for the refined microstructure in $BaTiO_3$ ceramics. Grain-boundaries pinned by second-phase precipitates and consequently their mobility reduced is also possible when the coarsening rate (dG/dt) is decreased. The enhanced sintering (Fig. 1) although achieved by ratio-control [23] is not completely due to the densification assisted by increased cation diffusivity (when the densification rate ($d\rho/dt$) is increased). Sintering in Y_2O_3-doped $BaTiO_3$ with Y_2O_3 higher than 0.80 mol%, presumably exceeded the solid solubility of Y_2O_3 in $BaTiO_3$, is improved by both enhanced densification (by solid-solution defect) and suppressed coarsening (by second-phase pinning) where the ($d\rho/dG$)-ratio is modified favourably.

4.2. Principal charge compensation mechanism

The charge compensation defects at temperatures higher than the lowest eutectic temperature (~1332 °C) must have contained electron in order to sustain the semiconductivity observed by Peng and Lu [1], Ting et al. [2], and Desu and Payne [24,25] in lightly donor-doped TiO_2-excess samples. That is not in accord with the preceding argument that cation vacancy is responsible for the sintering enhancement in donor-doped $BaTiO_3$.

The conductivity of $\sigma \approx 10^{-3}\,(\Omega\,\mathrm{mm})^{-1}$ for the 0.15 mol% La_2O_3-doped samples of $G_{av} = 15$–20 μm was attributed to electron compensation [1]. However, electron as the principal charge compensation defect is not conceivable for samples added with 0.15–0.80 mol% Y_2O_3 and laser-sintered at 1215 °C (lower than 1332 °C) since a refined microstructure (Fig. 2b) with low conductivity of $\sigma \approx 10^{-8}\,(\Omega\,\mathrm{mm})^{-1}$ was obtained (Fig. 5a). Changing of the principal charge compensation mechanism from vacancy to electron when the sintering temperature is increased from 1215 to 1350 °C must have occurred to account for the room-temperature conductivity, as shown in Fig. 5a and b. In fact, it has long been recognised [7,24] that the electrical properties of doped polycrystalline $BaTiO_3$ at room temperature are influenced by the defect structure. Room-temperature conductivity depends on the chemical compositions (e.g. nonstoichiometry and donor-levels), heat-treatment schedule, grain-size, and most importantly the effective quenching temperature below which the point defects are "frozen-in". Hence, the conductivity at room temperature is determined by how much the high-temperature defect structure has been retained metastably after cooling to room temperature.

It was suggested [3,7] that barium vacancies at high temperature equilibrium concentrating on grain surface diffuse towards the grain interior during cooling to room temperature. The oxidative cooling of TiO_2-excess $BaTiO_3$ ceramics further supported [10] the outward diffusion of Ba^{2+} to grain surface. The metastable retention of high-temperature defect structure is then determined by the time allowed for Ba^{2+}-diffusion to restore equilibrium at lower temperatures during cooling from sintering temperatures.

Restoration from the metastable high-temperature defect structure to the room-temperature defect equilibrium is elaborated below.

4.3. Restoration to room-temperature defect equilibrium

The time (τ) required for barium vacancy to diffuse from sintered grain surface to its interior can also be calculated using the following equation [3,7],

$$\tau \approx \frac{G_{av}^2}{D_{V''_{Ba}}} \tag{1}$$

where G_{av} is average grain-size, and $D_{V''_{Ba}}$ is lattice diffusion coefficient via barium vacancy.

Table 1
Calculated values of the time required for sintered $BaTiO_3$ ceramics to restore to its room-temperature equilibrium defect structure

T (°C)	$D_{V''_{Ba}}$ ($cm^2\ s^{-1}$)	τ (s)		
		G_{av} = 1 μm	G_{av} = 10 μm	G_{av} = 20 μm
1500	9.6×10^{-10}	10	1000	4300
1400	3.2×10^{-10}	31	3100	12500
1300	9.6×10^{-11}	100	1.0×10^4	4.2×10^4
1200	2.4×10^{-12}	417	4.2×10^4	1.7×10^5
1100	5.0×10^{-12}	2000	2.0×10^5	8.0×10^5
1000	8.0×10^{-13}	13000	1.3×10^6	5.0×10^6

$D_{V''_{Ba}} \approx 6.8 \times 10^{-2} \exp(-2.76\ \text{eV}/kT)\ \text{cm}^2\ \text{s}^{-1}$ has been determined experimentally by Daniels [7], where k is Boltzmann's constant of $8.61 \times 10^{-7}\ \text{eV K}^{-1}$, and T is absolute temperature (K).

Table 1 gives the time, calculated using Eq. (1), required for sintered $BaTiO_3$ ceramic to restore to its room-temperature equilibrium defect structure through the outward diffusion of Ba^{2+} via barium vacancies. For an average grain-size of ≤1 μm, barium diffusion is completed within 31 to 417 s (~7 min) for cooling from the sintering temperatures of 1200–1400 °C. Furnace cooling, however, often requires several hours to reach room temperature. That implies if samples added with donor oxides exceeding GGIT are sintered at 1200–1400 °C and (so) grain growth suppressed to $G_{av} \approx 1$ μm (e.g. Fig. 2b) they would become insulators after furnace cooling to room temperature. Since the insulating grain-boundary layer of approximately 1–3 μm thick was estimated [7] and such slow cooling rates would have completed the barium diffusion in every $BaTiO_3$ grain and restored to the room-temperature defect equilibrium. Indeed, it is often found in pressureless-sintering [1,2] that insulator $BaTiO_3$ ceramics was produced from furnace (slow-) cooling while semiconductivity retained in air-quenched samples of similar average grain-size (with doping levels >GGIT), and in which refined microstructure was obtained (e.g. Figs. 2b and 5a).

Others such as laser-sintered samples also showed the conductivity $\sigma = 10^{-3}$ to $10^{-4}\ (\Omega\ \text{mm})^{-1}$ (referred to Fig. 5a) when G_{av} was smaller than 1 μm for samples containing Y_2O_3-content exceeding GGIT (of 0.40 mol%) and sintering at 1325–1425 °C (Fig. 4). The indication is clearly that high-temperature defect equilibrium containing electron as the principal charge compensation defect is retained metastably to room temperature by faster cooling rates, such as that of air-quenching from laser-sintering, preventing any significant barium diffusion inwards to grain interior. The reason for the abrupt reduction of conductivity at T_1 = 1265 °C (Fig. 5a) is that the principal charge compensation mechanism has altered to predominantly vacancy, consistent with the schemes proposed by both Daniels and Wernicke. Therefore, laser-sintered samples may represent the high-temperature defect structure in $BaTiO_3$, as indicated by the higher conductivity (by ~10^5 from previous results). Further, T_1, T_2 derived from Fig. 5a and T_3, T_4 from Fig. 5b may also represent the transition temperatures of the principal charge compensation mechanism, i.e. electron compensation changes to a mixed mode at T_4 and then changes to (barium) vacancy compensation at T_3.

In fact, only fast cooled samples exhibit blue colour, indicating semiconductivity, while slowly cooled ones yellowish to brownish buff for doping levels exceeding GGIT. Samples doped with 0.15 mol% Y_2O_3, below GGIT, with $G_{av} \approx 12$ μm (Fig. 4) display blue in colour and give a conductivity $\sim 10^{-2}\ (\Omega\ \text{mm})^{-1}$ (Fig. 5a) when they were laser-sintered and air-quenched from 1350 °C. In contrast, samples pressureless-sintered at 1350 °C and furnace-cooled became less conductive of $\sigma \approx 10^{-10}\ (\Omega\ \text{mm})^{-1}$ [1]. The latter being furnace-cooled has allowed ample time for vacancy diffusion and restoration to the room-temperature defect equilibrium to complete (thus produced an insulator).

When Y^{3+} substitutes for both the A- and B-sites in $BaTiO_3$ [8,19], the Y^{3+}-site occupancy affect the final conductivity in the sintered ceramic. It is because substituting for the B-site, Y^{3+} becomes an acceptor-cation and so self-compensating [1,4,19]. Its effect on conductivity is more pronounced when samples are pressureless-sintered at 1300 °C for 15 h prior to laser-annealing, which has allowed for better dissolution of Y^{3+} and (so) resulted in lower conductivity due to self-compensation (as registered by data from higher doping levels of 0.80 and 1.0 mol%). Laser-annealed samples (Fig. 5b) indeed gave lower conductivity, where the discontinuity in region (II) at 1365 °C for highly Y_2O_3-doped, laser-sintered samples (the lower line in Fig. 5a) also disappears.

Three charge compensation schemes consistent with those proposed by Daniels [7] and Wernicke [3] also exist in Y_2O_3-doped TiO_2-excess $BaTiO_3$:

(III)	$T > 1500$ °C (T_4)	$N_D \approx n$	Electron compensation
(II)	1210 °C (T_3) $< T <$ 1500 °C (T_4)	$N_D = 2[V''_{Ba}] + n$	Mixed mode
(I)	$T <$ 1210 °C (T_3)	$N_D \approx 2[V''_{Ba}]$	Vacancy compensation

5. Conclusions

Grain-growth inhibition threshold occurs at ~0.40 mol% Y_2O_3 when the refined microstructure of an average grain size of ≈1 μm is obtained from solid-state sintering at 1215 °C. The principal charge compensation mechanism changing with temperature in the Y_2O_3-doped TiO_2-excess $BaTiO_3$ can be divided into three characteristic regimes. It altering from predominantly vacancy to a mixed mode and then to predominantly electron compensation occurring respectively at 1210 and 1500 °C has been identified experimentally from electrical conductivity measurement.

Acknowledgement

Funding of this research by the National Science Council of Taiwan through NSC-80-0405-E-110-018, 82-0405-E-110-029 and 83-0405-E-110-007 is acknowledged.

References

[1] C.J. Peng, H.Y. Lu, Compensation effect in semiconducting $BaTiO_3$, J. Am. Ceram. Soc. 71 (1) (1988) C44–C46.
[2] C.J. Ting, C.J. Peng, H.Y. Lu, S.T. Wu, Lanthanum–magnanese donor–acceptor-codoped semiconducting barium titanate, J. Am. Ceram. Soc. 73 (2) (1990) 329–334.
[3] R. Wernicke, The influence of kinetics processes on the electrical conductivity of donor-doped $BaTiO_3$ ceramics, Phys. Status Solidi A47 (1978) 39–44.
[4] L.A. Xue, Additives and the Control of Grain Growth in Barium Titatate Ceramics. Ph.D. thesis, University of Leeds, England, 1987.
[5] K.W. Kirby, B.A. Weschler, Phase relations in the barium–titanium oxide system, J. Am. Ceram. Soc. 74 (8) (1990) 841–847.
[6] M.H. Lin, J.F. Chou, H.Y. Lu, The rate-determining mechanism in the sintering of undoped non-stoichiometric barium titanate, J. Eur. Ceram. Soc. 20 (2000) 517–526.
[7] J. Daniels, Defect chemistry and electrical conductivity of doped barium titanate ceramics, Part II. Defect equilibrium acceptor-doped barium titanate, Philips Res. Rep. 31 (Part 2) (1976) 505–515.
[8] Y.M. Chiang, T. Takagi, Grain-boundary chemistry of barium titanate and strontium titanate: I. High temperature equilibrium space charge, J. Am. Ceram. Soc. 73 (11) (1990) 3278–3285.
[9] G.V. Lewis, C.R.A. Catlow, Computer modelling of barium titanate, Radiation Effect 73 (1–4) (1983) 307–314.
[10] A. Yamada, Y.M. Chiang, Nature of cation vacancies formed to compensate donor during oxidation of barium titanate, J. Am. Ceram. Soc. 78 (4) (1995) 909–914.
[11] M.H. Lin, H.Y. Lu, Densification retardation in the sintering of La_2O_3-doped barium titanate ceramics, Mater. Sci. Eng. A323 (2002) 167–176.
[12] M.I. Mendelson, Average grain size in polycrystalline ceramics, J. Am. Ceram. Soc. 52 (8) (1969) 443–446.
[13] H. Schmelz, A. Meyer, The evidence for anomalous grain growth below the eutectic temperature in $BaTiO_3$ ceramics, Ceram. Forum Int. 59 (1982) 436–440.
[14] O. Eibl, P. Pongratz, P. Skalicky, H. Schmelz, Formation of (1 1 1) twins in $BaTiO_3$ ceramics, J. Am. Ceram. Soc. 70 (8) (1987) 195–197.
[15] D.F.K. Hennings, R. Janssen, P.J.L. Reynen, Control of liquid-phase-enhanced discontinuous grain growth in barium titanate, J. Am. Ceram. Soc. 70 (1) (1987) 23–27.
[16] J.H. Hwang, Y.H. Han, Dielectric properties of erbium doped barium titanate, Jpn. J. Appl. Phys. 40 (Part 12A) (2001) 676–679.
[17] R.J. Brook, Controlled grain growth. Ceramic fabrication processes, in: F.F.Y. Wang (Ed.), Treatise on Materials Science and Technology, vol. 9, Academic Press, New York, 1976, pp. 331–364.
[18] P. Blanchart, J.F. Baumard, P. Abelard, Effects of yttrium doping on the grain and grain-boundary resistivities of $BaTiO_3$ for positive temperature coefficient thermistors, J. Am. Ceram. Soc. 75 (5) (1992) 1068–1072.
[19] J. Zhi, A. Chen, Y. Zhi, P.M. Vilarinho, J.L. Baptista, Incorporation of ytterium in barium titanate ceramics, J. Am. Ceram. Soc. 82 (5) (1999) 1345–1348.
[20] M.H. Lin, H.Y. Lu, Site occupancy of ytterium as dopant cation in BaO-excess $BaTiO_3$, Mater. Sci. Eng. A335 (1/2) (2002) 101–108.
[21] Y. Tsur, A. Hitomi, I. Scrymgeour, C.A. Randall, Site occupancy of rare-earth cations in $BaTiO_3$, Jpn. J. Appl. Phys. 40 (Part 1, 1) (2001) 255–258.
[22] T.F. Lin, C.T. Hu, I.N. Lin, Defects restoration during cooling and annealing in PTC type barium titanate ceramics, J. Mater. Sci. 25 (1990) 3029–3033.
[23] R.J. Brook, Fabrication principle for the production of ceramics with superior mechanical properties, Proc. Br. Ceram. Soc. 32 (3) (1982) 7–24.
[24] S.B. Desu, D.A. Payne, Interfacial segregation in perovskites: II. Experimental evidence, J. Am. Ceram. Soc. 73 (11) (1990) 3398–3406.
[25] S.B. Desu, D.A. Payne, Interfacial segregation in perovskites: III. Microstructure and electrical properties, J. Am. Ceram. Soc. 73 (11) (1990) 3407–3415.